Conductive heat transfer in a rarefied polyatomic gas confined between coaxial cylinders

Christos Tantos [a], Dimitris Valougeorgis [a,*], Marco Pannuzzo [b], Aldo Frezzotti [b], Gian Luca Morini [c]

[a] Department of Mechanical Engineering, University of Thessaly, Pedion Areos, 38334 Volos, Greece
[b] Dipartimento di Scienze & Tecnologie Aerospaziali, Politecnico di Milano, Via La Masa, 34, 20156 Milano, Italy
[c] DIENCA, Università degli Studi di Bologna, Via Risorgimento 2, 40136 Bologna, Italy

ABSTRACT

The conductive heat transfer through rarefied gases composed by rigid rotators and confined between coaxially placed cylinders maintained at different temperatures is investigated on the basis of the Holway and Rykov kinetic models as well as on the Boltzmann equation via the DSMC scheme supplemented by the Borgnakke–Larsen collision model. The translational and rotational parts as well as the total temperature and heat flux distributions are computed and their behavior in terms of the gas rarefaction, the temperature difference between the cylinders and the ratio of the radii is investigated. The two kinetic models and the DSMC method provide results which are in good agreement for HS and VHS molecules. Furthermore, very good agreement with available experimental data for polyatomic gases has been observed at small and large temperature differences validating the implemented modeling. Qualitatively the behavior of the dimensionless total macroscopic quantities is similar to that of the monatomic ones. Quantitatively however, the heat fluxes of polyatomic gases are significantly higher than the corresponding monatomic ones. Also, as the amount of the elastic compared to the inelastic collisions is increased, the translational heat fluxes are increased and they tend to the monatomic ones, while always the rotational heat fluxes are about 50% and 75% of the translational ones for linear and non-linear rigid rotators, respectively. It is clearly demonstrated that heat transfer simulations through rarefied polyatomic gases in MEMS and other devices cannot rely on typical monatomic modeling. On the contrary, reliable kinetic modeling for polyatomic gases must be implemented.

1. Introduction

The classical problem of heat conduction through a stationary rarefied gas confined between concentric cylinders maintained at different temperatures, which has been used to determine the thermal conductivity of gases and the energy accommodation at the inner cylinder has been recently attracted a renewed interest. This is due to potential applications in several emerging technological fields including micro heat exchangers and micro sensors in microfluidics, pressure gauges in vacuum technology, multilayer insulation blankets in space vehicles and cryogenic systems. The case of heat transfer through a monatomic gas has been extensively investigated. The literature survey on this topic is very long and only some very recent papers for linear and nonlinear kinetic treatment of single monatomic gases or mixtures of monatomic gases are cited here [1–4]. However, the research work is not as

extensive in the case of polyatomic gases, where the contribution of the internal degrees of freedom to thermal effects is expected to be important, leading to deviations from the corresponding monatomic results.

The polyatomic kinetic models by Morse [5], Holway [6] and Hanson and Morse [7] have been implemented to solve the plane heat transfer and temperature jumps problems. Most of the work refers to small temperature differences and the applied linearized kinetic model equations are solved via semi-analytical techniques and variational methods [8–11] as well as by an early version of the discrete ordinates (velocity) method [12]. The model proposed by Rykov [13] has also been implemented to solve heat transfer in diatomic gases confined between parallel plates in a wide range of temperatures providing good agreement with experimental data [14]. Also, experimental work in polyatomic gases between parallel plates has been performed in [15–17] measuring heat flow rates and thermal accommodation coefficients respectively.

The available research work of cylindrical heat conduction in rarefied polyatomic gases is rather limited. There are only the early

works of Lees and Liu [18] applying the "two-sided Maxwellian" associated with the 4th order moment method and of Cipolla and Morse [19] solving the Morse model by the "Knudsen iteration scheme" for small temperature differences. Experimental work has been performed for very small temperature differences in [20] and for larger differences in [21,22]. The two latter works have direct relevance to the design of evacuated solar collectors and Pirani micro sensors respectively. In [21], the DSMC method [23] subject to the Borgnakke-Larsen collision scheme [24] has also been applied to provide satisfactory data for desorbable gases which are difficult to obtain experimentally.

Thus, a detailed investigation of the conductive heat transfer through rarefied polyatomic gases confined between two coaxially placed cylinders is needed and it is tackled in the present work considering only rotational degrees of freedom. This heat transfer configuration is investigated here, based on both deterministic and stochastic methodologies. The deterministic modeling includes the direct solution of the Holway and Rykov models, whereas the stochastic DSMC scheme is adopted to solve the Boltzmann equation in combination with the Borgnakke-Larsen collision model. Macroscopic quantities are provided for various radii ratios in a wide range of the Knudsen number and for small, moderate and large temperature differences. Comparisons between kinetic models and DSMC results as well as between simulations and available in the literature experimental data are presented and discussed. The validity of the results is confirmed and the effects of all involved parameters on the heat flux and on the temperature and density distributions are examined. Also, the influence of the number of rotational degrees of freedom is investigated and the differences (and similarities) compared to the corresponding monatomic gas heat transfer problem are pointed out.

2. Heat transfer configuration

Consider two concentric stationary cylinders with radii R_A, R_B and the annular gap $\Re = \{(x,y): R_A^2 < x^2 + y^2 < R_B^2\}$ filled with a polyatomic gas at rest and arbitrary density level. The temperature of the inner and outer cylinder are maintained constant at T_A and T_B respectively with $T_A > T_B$. The cylinders are assumed to be very long and variations in the axial direction (end effects) are neglected. Then, due to the temperature difference there is an axisymmetric conductive heat flow through the gas from the inner hot cylinder towards the cold outer cylinder.

In the temperature range where the effects of vibrational degrees of freedom can be neglected, the problem may be modeled by the Boltzmann equation for a gas of rigid rotators. When, as in the case considered here, intrinsic molecular angular momenta (spin) have no preferential alignment, it is reasonable to describe molecular internal states through a single variable, the internal energy I or the angular momentum modulus. Then, the gas is described by a spin orientation averaged distribution function $f(\hat{r}, v, I, t)$, which obeys the following kinetic equation [25]:

$$\frac{\partial f}{\partial t} + v \frac{\partial f}{\partial \hat{r}} = \int \left[f(\hat{r}, v_1', I_1', t) f(\hat{r}, v', I', t) - f(\hat{r}, v_1, I_1, t) f(\hat{r}, v, I, t) \right]$$
$$\times Q I_1^\mu d^3 v_1 dI_1 \qquad (1)$$

In Eq. (1), t denotes time, $v = (v_r, v_\vartheta, v_z) = (\xi \cos \theta, \xi \sin \theta, v_z)$ is the molecular velocity ($v^2 = \xi^2 + v_z^2$) and $\hat{r} = (\hat{r}, \vartheta)$ is the position vector, while Q is defined as

$$Q = \int_S d^2 \hat{e}' \int_0^{E-I'} I'^\mu dI' \int_0^{E-I_1'} I_1'^\mu dI_1 \frac{v_r'^2}{v_r} \sigma(E; \hat{e}' \circ \hat{e}; I', I_1' \to I, I_1) \qquad (2)$$

Here, $\sigma(E; \hat{e}' \circ \hat{e}; I', I_1' \to I, I_1)$ is the differential cross-section associated with a binary collision, which produces a pair of molecules in the final states (v, I), (v_1, I_1) from a pair of molecules in the initial

states (v', I'), (v_1', I_1'). The argument E denotes the conserved total energy in the center of mass reference frame:

$$E = \frac{1}{4} m v_r^2 + I + I_1 = \frac{1}{4} m v_r'^2 + I' + I_1' \qquad (3)$$

The unit vectors $\hat{e}' = v_r'/v_r'$ and $\hat{e} = v_r/v_r$ have the directions of the relative velocities $v_r' = v_1' - v'$ and $v_r = v_1 - v$ before and after a collision, respectively. The exponent μ in Eq. (1) takes the values 0 for $j = 2$ and $1/2$ for $j = 3$, with j being the number of rotational degrees of freedom.

The main parameters characterizing this problem are the dimensionless temperature difference

$$\beta = \frac{T_A - T_B}{T_B} = \frac{\Delta T}{T_B} \qquad (4)$$

the ratio of the inner over the outer radius

$$\gamma = \frac{R_A}{R_B} \qquad (5)$$

and the reference gas rarefaction parameter

$$\delta_B = \frac{R_B P_B}{\mu_B \upsilon_B} \qquad (6)$$

In the latter expression P_B is a reference gas pressure, measured when the system is in equilibrium ($T_A = T_B$), μ_B is the gas viscosity at reference temperature T_B and $\upsilon_B = \sqrt{2 k_B T_B / m}$, with k_B being the Boltzmann constant and m the molecular mass, is the most probable molecular speed. The gas rarefaction parameter is proportional to the inverse of the Knudsen number and the cases of $\delta_B = 0$ and $\delta_B \to \infty$ correspond to the free molecular and hydrodynamic limits respectively.

The problem is axially symmetric and one-dimensional in the physical space $R_A < \hat{r} < R_B$. The macroscopic quantities of practical interest are the number density distribution

$$n(\hat{r}) = \int_0^{2\pi} \int_0^\infty \int_{-\infty}^\infty \int_0^\infty f dI dv_z \xi d\xi d\theta \qquad (7)$$

as well as the temperature and heat flux distributions denoted by $T(\hat{r})$ and $Q(\hat{r})$ respectively. In polyatomic gases the internal energy can be divided in two parts, the energy of the translational motion and the energy associated to the internal structure. These energies are related to the corresponding temperatures and heat fluxes. Then, the translational, rotational and total (thermodynamic) temperatures are:

$$T_{tr}(\hat{r}) = \frac{m}{3 k_B n} \int_0^{2\pi} \int_0^\infty \int_{-\infty}^\infty \int_0^\infty (\xi^2 + v_z^2) f dI dv_z \xi d\xi d\theta \qquad (8)$$

$$T_{rot}(\hat{r}) = \frac{2}{j k_B n} \int_0^{2\pi} \int_0^\infty \int_{-\infty}^\infty \int_0^\infty f I dI dv_z \xi d\xi d\theta \qquad (9)$$

$$T(\hat{r}) = \frac{3 T_{tr}(\hat{r}) + j T_{rot}(\hat{r})}{3 + j} \qquad (10)$$

The subscripts *tr* and *rot* refer to translational and rotational parts respectively, with $j = 2$ for diatomic and linear molecules and $j = 3$ in all other cases (nonlinear molecules). The corresponding heat fluxes are:

$$Q_{tr}(\hat{r}) = \frac{m}{2} \int_0^{2\pi} \int_0^\infty \int_{-\infty}^\infty \int_0^\infty (\xi^2 + v_z^2)(\xi \cos \theta) f dI dv_z \xi d\xi d\theta \qquad (11)$$

$$Q_{rot}(\hat{r}) = \int_0^{2\pi} \int_0^\infty \int_{-\infty}^\infty \int_0^\infty (\xi \cos \theta) f I dI dv_z \xi d\xi d\theta \qquad (12)$$

$$Q(\hat{r}) = Q_{tr}(\hat{r}) + Q_{rot}(\hat{r}) \qquad (13)$$

Here, the effect of all involved parameters, namely of β, γ and δ_B on the heat flux, temperature and density distributions for diatomic and polyatomic gases is examined. This is achieved both in a

deterministic and stochastic manner described in Sections 3 and 4 respectively. The former approach includes the replacement of the rather complex collision term of Eq. (1) by the Holway and Rykov kinetic models, while the latter one the implementation of the DSMC method.

3. Deterministic kinetic modeling

The effort of solving Eq. (1) either analytically or numerically, is significantly reduced by substituting its collision term with reliable kinetic models. Two classical kinetic models, which have been commonly applied with considerable success in rarefied polyatomic gas flows and heat transfer configurations providing good agreement with experimental results, are the models introduced by Holway [6] and Rykov [13]. They may be considered as BGK type models and, for monatomic gases they are reduced to the BGK [26] (or the ES [27,6]) model and to the Shakhov [28] model respectively. The H-theorem has been proven for a polyatomic gas in the case of the Holway model [29], while such proof is not available for the Rykov (and Shakhov) models. In the present work for purposes related mainly to benchmarking and validation of results both the Holway and Rykov models are applied. The Rykov model is applicable only to diatomic gases ($j = 2$), while the Holway model is more general and is applicable to polyatomic gases as well ($j = 2,3$).

Both models for the present steady-state heat transfer configuration can be written in a similar form as [6,13]

$$\xi \cos\theta \frac{\partial f^{(i)}}{\partial \hat{r}} - \frac{\xi \sin\theta}{\hat{r}} \frac{\partial f^{(i)}}{\partial \theta} = v_{rot}^{(i)}\left(f_{rot}^{(i)} - f^{(i)}\right) + v_{tr}^{(i)}\left(f_{tr}^{(i)} - f^{(i)}\right) \quad (14)$$

where the superscript $i = H,R$ denotes the Holway (H) and Rykov (R) models respectively. Here, the collision term consists of the elastic and inelastic collision parts, with the subscripts tr referring to elastic and rot to inelastic. The quantities $v_{tr}^{(i)}$ and $v_{rot}^{(i)}$ denote the frequency of the elastic and inelastic collisions respectively, while $f_{tr}^{(i)}$ and $f_{rot}^{(i)}$ are the corresponding relaxing distributions.

It is obvious that the dependency of the distribution function $f^{(i)}, i = H,R$ to the energy I of the rotational motion significantly increases the computational effort compared to the monatomic gas case. It turns out however, that for BGK type models all macroscopic quantities can be obtained by a simpler formalism introducing two reduced density distributions one for the mass and one for the internal energy according to $\hat{g} = \int_{-\infty}^{\infty} f dI$ and $\hat{h} = \int_{-\infty}^{\infty} f I dI$ [13,29,30]. Then, by integrating Eq. (14) in dI and $I dI$ yields the equations

$$\xi \cos\theta \frac{\partial \hat{g}^{(i)}}{\partial \hat{r}} - \frac{\xi \sin\theta}{\hat{r}} \frac{\partial \hat{g}^{(i)}}{\partial \theta} = v_{rot}^{(i)}\left(\hat{g}_{rot}^{(i)} - \hat{g}^{(i)}\right) + v_{tr}^{(i)}\left(\hat{g}_{tr}^{(i)} - \hat{g}^{(i)}\right) \quad (15)$$

$$\xi \cos\theta \frac{\partial \hat{h}^{(i)}}{\partial \hat{r}} - \frac{\xi \sin\theta}{\hat{r}} \frac{\partial \hat{h}^{(i)}}{\partial \theta} = v_{rot}^{(i)}\left(\hat{h}_{rot}^{(i)} - \hat{h}^{(i)}\right) + v_{tr}^{(i)}\left(\hat{h}_{tr}^{(i)} - \hat{h}^{(i)}\right) \quad (16)$$

which are coupled through the macroscopic quantities appearing in the relaxing distributions. At this stage the following dimensionless quantities are introduced ($i = H,R$):

$$r = \frac{\hat{r}}{R_B}, \quad \zeta = \frac{\xi}{v_B}, \quad c_z = \frac{v_z}{v_B}, \quad g^{(i)} = \frac{\hat{g}^{(i)} v_B^3}{n_B}, \quad h^{(i)} = \frac{\hat{h}^{(i)} v_B^3}{P_B}$$

$$\rho^{(i)} = \frac{n^{(i)}}{n_B}, \quad \tau_{tr}^{(i)} = \frac{T_{tr}^{(i)}}{T_B}, \quad \tau_{rot}^{(i)} = \frac{T_{rot}^{(i)}}{T_B}, \quad \tau^{(i)} = \frac{3\tau_{tr}^{(i)} + j\tau_{rot}^{(i)}}{3+j}$$

$$q_{tr}^{(i)} = \frac{Q_{tr}^{(i)}}{P_B v_B}, \quad q_{rot}^{(i)} = \frac{Q_{rot}^{(i)}}{P_B v_B}, \quad q^{(i)} = q_{tr}^{(i)} + q_{rot}^{(i)} \quad (17)$$

All quantities with the subscript B are considered as reference quantities ($P_B = n_B k_B T_B$). Here, $g^{(i)} = g^{(i)}(r,\zeta,\theta,c_z)$ and $h^{(i)} = h^{(i)}(r,\zeta,\theta,c_z)$ are the dimensionless distributions, with $\gamma \leqslant r \leqslant 1$ while $\mathbf{c} = (\zeta\cos\theta, \zeta\sin\theta, c_z)$ is the dimensionless molecular velocity vector. Furthermore, $\rho^{(i)}$, $\tau^{(i)}$ and $q^{(i)}$ are the dimensionless distributions of number density, temperature and radial heat flux respectively, with $\tau_{tr}^{(i)}, \tau_{rot}^{(i)}, q_{tr}^{(i)}$,

$q_{rot}^{(i)}$ denoting the corresponding dimensionless translational and rotational parts.

Next, the computational effort is further reduced by eliminating the c_z component of the molecular velocity by introducing the reduced distributions:

$$F^{(i)} = \int_{-\infty}^{\infty} g^{(i)} dc_z \quad G^{(i)} = \int_{-\infty}^{\infty} g^{(i)} c_z^2 dc_z \quad S^{(i)} = \int_{-\infty}^{\infty} h^{(i)} dc_z \quad (18)$$

By operating successively on Eq. (15) with the integral operators $\int(.)dc_z$ and $\int(.)c_z^2 dc_z$ as well as on Eq. (16) with $\int(.)dc_z$, a system of three integro-differential equations are obtained, which in compact vector form is written as

$$\zeta \cos\theta \frac{\partial \mathbf{\Psi}^{(i)}}{\partial r} - \frac{\zeta \sin\theta}{r} \frac{\partial \mathbf{\Psi}^{(i)}}{\partial \theta}$$
$$= \delta_B \rho^{(i)} \left(\tau_{tr}^{(i)}\right)^{1-\omega} \mathrm{Pr}^\alpha \left[\frac{1}{Z}\left(\mathbf{\Psi}_{rot}^{(i)} - \mathbf{\Psi}^{(i)}\right) + \left(1 - \frac{1}{Z}\right)\left(\mathbf{\Psi}_{tr}^{(i)} - \mathbf{\Psi}^{(i)}\right)\right] \quad (19)$$

Here, the vector of the unknown distributions $\mathbf{\Psi}^{(i)} = [F^{(i)}, G^{(i)}, S^{(i)}]^T$ depends on three independent variables, namely r, ζ and θ. Also, the reference gas rarefaction δ_B is given by Eq. (6), Pr is the Prandtl number of the gas, with the parameter $\alpha = 1$ in the Holway model ($i = H$) and $\alpha = 0$ in the Rykov model ($i = R$), while the parameter $1 \leqslant Z < \infty$ indicates the fraction of rotational collisions with regard to the total collisions. As $Z \to \infty$, the first two equations in (19) for $i = H,R$ are transformed to the corresponding reduced BGK and Shakhov equations for monatomic gas. In the derivation of Eq. (19) the Inverse Power Law (IPL) interaction between particles has been introduced with $\omega \in [0.5,1]$. In addition, the translational and rotational relaxing distributions in Eq. (19) are given by $\mathbf{\Psi}_{tr}^{(i)} = \left[F_{tr}^{(i)}, G_{tr}^{(i)}, S_{tr}^{(i)}\right]^T$ and $\mathbf{\Psi}_{rot}^{(i)} = \left[F_{rot}^{(i)}, G_{rot}^{(i)}, S_{rot}^{(i)}\right]^T$ respectively, where the components of these vectors for each kinetic model are as follows:

(i) H-model

$$F_{tr}^{(H)} = \frac{\rho^{(H)}}{\pi \tau_{tr}^{(H)}} exp\left[-\zeta^2/\tau_{tr}^{(H)}\right] \quad G_{tr}^{(H)} = \frac{1}{2}\tau_{tr}^{(H)} F_{tr}^{(H)} \quad S_{tr}^{(H)} = \frac{j}{2}\tau_{rot}^{(H)} F_{tr}^{(H)}$$

$$F_{rot}^{(H)} = \frac{\rho^{(H)}}{\pi \tau^{(H)}} exp\left[-\zeta^2/\tau^{(H)}\right] \quad G_{rot}^{(H)} = \frac{1}{2}\tau^{(H)} F_{rot}^{(H)} \quad S_{rot}^{(H)} = \frac{j}{2}\tau^{(H)} F_{rot}^{(H)} \quad (20)$$

(ii) R-model

$$F_{tr}^{(R)} = \frac{\rho^{(R)}}{\pi \tau_{tr}^{(R)}} exp\left[-\frac{\zeta^2}{\tau_{tr}^{(R)}}\right]\left[1 + \frac{4}{15}\frac{q_{tr}^{(R)}\zeta\cos\theta}{\rho^{(R)}\left(\tau_{tr}^{(R)}\right)^2}\left(\frac{\zeta^2}{\tau_{tr}^{(R)}} - 2\right)\right]$$

$$G_{tr}^{(R)} = \frac{1}{2}\frac{\rho^{(R)}}{\pi} exp\left[-\frac{\zeta^2}{\tau_{tr}^{(R)}}\right]\left[1 + \frac{4}{15}\frac{q_{tr}^{(R)}\zeta\cos\theta}{\rho^{(R)}\left(\tau_{tr}^{(R)}\right)^2}\left(\frac{\zeta^2}{\tau_{tr}^{(R)}} - 1\right)\right]$$

$$S_{tr}^{(R)} = \frac{\rho^{(R)}\tau_{rot}^{(R)}}{\pi \tau_{tr}^{(R)}} exp\left[-\frac{\zeta^2}{\tau_{tr}^{(R)}}\right]\left[1 + \frac{4}{15}\frac{q_{tr}^{(R)}\zeta\cos\theta}{\rho^{(R)}\left(\tau_{tr}^{(R)}\right)^2}\left(\frac{\zeta^2}{\tau_{tr}^{(R)}} - 2\right)\right.$$
$$\left. + 2(1-\kappa)\frac{q_{rot}^{(R)}\zeta\cos\theta}{\rho^{(R)}\tau_{tr}^{(R)}\tau_{rot}^{(R)}}\right]$$

$$F_{rot}^{(R)} = \frac{\rho^{(R)}}{\pi \tau^{(R)}} exp\left[-\frac{\zeta^2}{\tau^{(R)}}\right]\left[1 + \omega_0 \frac{4}{15}\frac{q_{tr}^{(R)}\zeta\cos\theta}{\rho^{(R)}(\tau^{(R)})^2}\left(\frac{\zeta^2}{\tau^{(R)}} - 2\right)\right]$$

$$G_{rot}^{(R)} = \frac{1}{2}\frac{\rho^{(R)}}{\pi} exp\left[-\frac{\zeta^2}{\tau^{(R)}}\right]\left[1 + \omega_0 \frac{4}{15}\frac{q_{tr}^{(R)}\zeta\cos\theta}{\rho^{(R)}(\tau^{(R)})^2}\left(\frac{\zeta^2}{\tau^{(R)}} - 1\right)\right]$$

$$S_{rot}^{(R)} = \frac{\rho^{(R)}}{\pi} exp\left[-\frac{\zeta^2}{\tau^{(R)}}\right]\left[1 + \omega_0 \frac{4}{15}\frac{q_{tr}^{(R)}\zeta\cos\theta}{\rho^{(R)}(\tau^{(R)})^2}\left(\frac{\zeta^2}{\tau^{(R)}}-2\right)\right.$$
$$\left. + 2\omega_1(1-\kappa)\frac{q_{rot}^{(R)}\zeta\cos\theta}{\rho^{(R)}(\tau^{(R)})^2}\right] \tag{21}$$

It is stated in [31] that the parameters ω_0 and ω_1 are chosen so that the thermal conductivity obtained from the model equation is close to the experimental data in [32]. It is also pointed that the parameter κ for a power intermolecular potential is constant.

The macroscopic quantities in Eqs. (19)–(21) in terms of the reduced distributions $F^{(i)}, G^{(i)}$ and $S^{(i)}$ are obtained by operating accordingly on Eqs. (7)–(13). A similar manipulation to the one applied in the governing equations is applied to deduce the following moments:

$$\rho^{(i)} = \frac{n^{(i)}}{n_B} = \int_0^{2\pi}\int_0^\infty F^{(i)}\zeta d\zeta d\theta \tag{22}$$

$$\tau_{tr}^{(i)} = \frac{T_{tr}^{(i)}}{T_B} = \frac{2}{3\rho^{(i)}}\int_0^{2\pi}\int_0^\infty \left(\zeta^2 F^{(i)}+G^{(i)}\right)\zeta d\zeta d\theta \tag{23}$$

$$\tau_{rot}^{(i)} = \frac{T_{rot}^{(i)}}{T_B} = \frac{2}{j\rho^{(i)}}\int_0^{2\pi}\int_0^\infty S^{(i)}\zeta d\zeta d\theta \tag{24}$$

$$\tau^{(i)} = \frac{3\tau_{tr}^{(i)}+j\tau_{rot}^{(i)}}{3+j} \tag{25}$$

$$q_{tr}^{(i)} = \frac{Q_{tr}^{(i)}}{P_B\upsilon_B} = \int_0^{2\pi}\int_0^\infty \left(\zeta^2 F^{(i)}+G^{(i)}\right)(\zeta\cos\theta)\zeta d\zeta d\theta \tag{26}$$

$$q_{rot}^{(i)} = \frac{Q_{rot}^{(i)}}{P_B\upsilon_B} = \int_0^{2\pi}\int_0^\infty S^{(i)}(\zeta\cos\theta)\zeta d\zeta d\theta \tag{27}$$

$$q^{(i)} = q_{tr}^{(i)}+q_{rot}^{(i)} \tag{28}$$

It is noted that by operating accordingly on Eq. (19) the conservation equations

$$\frac{\partial[rq^{(i)}(r)]}{\partial r} = 0 \tag{29}$$

are readily deduced, which imply that the products $rq^{(i)}(r)$ remain constant along $\gamma \leqslant r \leqslant 1$. Therefore in the Section 5, results for the heat fluxes are presented only at the inner hot cylinder where $r = \gamma$. In addition, these conservation equations are used for benchmarking purposes.

To close the problem formulation boundary conditions have to be assigned. Although the numerical formulation would allow more general wall scattering models, purely diffuse type boundary conditions are considered throughout the present work. Then, the outgoing distributions associated to Eq. (19) are at the inner wall ($r = \gamma$)

$$F^{(i)} = \frac{\rho_w^{(i)}}{\pi(1+\beta)}\exp\left[-\zeta^2/(1+\beta)\right] \quad G^{(i)} = \frac{1}{2}(1+\beta)F^{(i)} \quad S^{(i)}$$
$$= \frac{j}{2}(1+\beta)F^{(i)} \tag{30}$$

and at the outer wall ($r = 1$)

$$F^{(i)} = \frac{1}{\pi}\exp\left[-\zeta^2\right] \quad G^{(i)} = \frac{1}{2}F^{(i)} \quad S^{(i)} = \frac{j}{2}F^{(i)} \tag{31}$$

Boundary conditions (30) and (31) are valid for $\theta \in [-\pi/2, \pi/2]$ and $\theta \in [\pi/2, 3\pi/2]$ respectively. The density $\rho_w^{(i)}$, associated with the outgoing wall flux is obtained from the ingoing flux to obtain a zero wall net mass flux.

The nonlinear vector Eq. (19) along with the associated expressions 20 and 21, the moments (22)–(28) and the boundary conditions (30) and (31) provide a theoretically well-established closed kinetic formulation for the heat transfer problem under

consideration, which is solved numerically both for the Holway and Rykov models in a deterministic manner. The implemented numerical scheme is the same with the one described in [2] and therefore only a brief description is provided.

The molecular velocity space (ζ, θ), with $\zeta \in [0, \infty)$, $\theta \in [0, 2\pi]$, and the physical space $r \in [\gamma, 1]$ are discretized. The continuum spectrum of magnitudes of the molecular velocity vector is replaced by a set of discrete magnitudes $\zeta_m \in [0, \zeta_{max}]$, $m = 1, 2, \ldots, M$, which are taken to be the roots of the Legendre polynomial of order M accordingly mapped from $[-1, 1]$ to $[0, \zeta_{max}]$. Also, by using a uniform grid, the angular space is divided into N intervals. Each of the angular intervals is defined by its angle $\theta_n, n = 1, 2, \ldots, N$. Finally, the distance between the two cylinders is divided into K equal segments, defined by r_k, $k = 1, 2, \ldots, K+1$.

The integro-differential equation (19) are first discretized in the variable ζ and the resulting equations are integrated over each spatial and angular intervals $[r_{k-1/2}, r_{k+1/2}]$ and $[\theta_{n-1/2}, \theta_{n+1/2}]$. The moments (22)–(28) are numerically integrated by applying the trapezoidal rule and Gauss–Legendre quadrature in the polar angle θ and the velocity magnitude ζ respectively. The resulting discretized equations for $\Psi_{k,m,n}^{(i)} = [F_{k,m,n}^{(i)}, G_{k,m,n}^{(i)}, S_{k,m,n}^{(i)}]^T$ with the associated discretized moments are solved in an iterative manner which is concluded when the convergence criteria

$$\frac{1}{3(K+1)}\sum_{i=1}^{K+1}\left[\left|\rho_i^{(t+1)}-\rho_i^{(t)}\right|+\left|\tau_i^{(t+1)}-\tau_i^{(t)}\right|+\left|q_i^{(t+1)}-q_i^{(t)}\right|\right] < \varepsilon$$

with t denoting the iteration index, is fulfilled. The results presented in Section 5 have been obtained with $M = 24$, $N = 400$ and $K = 800$ for $\gamma \geqslant 0.1$ and $K = 2000$ for $\gamma < 0.1$, while the termination parameter is set to $\varepsilon = 10^{-8}$.

It is noted that upon convergence the conservation Eq. (29) is accordingly satisfied in several significant figures. In addition, the numerical solutions at the free molecular ($\delta_B = 0$) and continuum ($\delta_B \to \infty$) limits have an excellent agreement with the corresponding analytical ones presented in Appendix A.

4. Stochastic modeling: DSMC solutions of the Boltzmann equation

In order to increase confidence into the predictions of the kinetic models described in the previous section, the problem has also been studied by solving Eq. (1) by a DSMC particle scheme [23]. In general, the determination of the form of the collision cross section for polyatomic gases is not easy. As it is well known, the dynamics of a binary *molecular* collision is much more complicated than a binary *atomic* collision which is largely amenable to analytical treatment. Simple mechanical models of translational-rotational coupling (rough spheres, loaded spheres, spherocylinders) [33] are not flexible enough to fit experimental data on polyatomic species. Hence, the collision dynamics and cross-sections have been obtained from the well-known phenomenological model proposed by Borgnakke and Larsen [24]. The model can be easily adapted to reproduce experimental translational-rotational relaxation rates with good accuracy [34]. Moreover, its collision algorithm is very well suited to particle schemes used to obtain numerical solutions of the Boltzmann equation [23].

In the particular form of the Borgnakke-Larsen model adopted here, collision dynamics is organized as follows:

- The collision probability of two molecules in the pre-collision state (υ', I'), (υ_1', I_1') is proportional to $\sigma_{hs}\upsilon_r'$, where $\sigma_{hs} = \pi a^2$ is the integral cross-section of hard sphere molecules of diameter a and $\upsilon_r' = \|\upsilon_1' - \upsilon'\|$ is the relative velocity modulus.
- An individual collision is inelastic with probability $1/Z$ or elastic with probability $1 - 1/Z$. An inelastic collision gives rise to an

exchange between translational and rotational energies, as explained below. In an elastic collision pre- and post-collision rotational energies do not change, i.e. $I = I'$, $I_1 = I'_1$. Conservation of total energy then implies $v_r = v'_r$ and, according to hard sphere impact dynamics, post-collision relative velocity is written as $\boldsymbol{v}_r = v_r \hat{\boldsymbol{e}}$, being $\hat{\boldsymbol{e}}$ a random vector uniformly distributed on the unit sphere S.

- In an inelastic collision total energy E is randomly partitioned between translational and rotational motion by sampling the translational energy fraction E_{tr}/E from a given probability density function $P_1(E_{tr}/E|j)$. The available total rotational energy $E_{rot} = I + I_1 = E - E_{tr}$ is then randomly distributed between the collision partners by sampling the fraction I/E_{rot} from a given probability density function $P_2(I/E_{rot}|j)$. The relative velocity after a collision is again written as $\boldsymbol{v}_r = v_r \hat{\boldsymbol{e}}$, where $\hat{\boldsymbol{e}}$ is a random unit vector and $v_r = \sqrt{4E_{tr}/m}$.

The specific form of the probability densities $P_1(E_{tr}/E|j)$ and $P_2(I/E_{rot}|j)$ depends both on the number of internal degrees of freedom and on the assumed intermolecular interaction [23]. In the case of hard sphere interaction and $j = 2$ they take a particularly simple form [23,25]

$$P_1(E_{tr}/E|2) = 6\frac{E_{tr}}{E}\left(1 - \frac{E_{tr}}{E}\right) \tag{32}$$

$$P_2(I/E_{rot}|2) = 1 \tag{33}$$

As shown by Eq. (32), post-collision translational energy has a parabolic distribution; the available E_{rot} amount is then randomly divided between I and I_1, according to Eq. (33). Taking into account the assumed scattering isotropy and Eqs. (32) and (33) the collision cross-section takes the form:

$$\sigma\left(E; \hat{\boldsymbol{e}}' \circ \hat{\boldsymbol{e}}; I', I'_1 \to I, I_1\right) = \frac{\sigma_{hs}}{4\pi E^2}\theta\left(I, I_1, I', I'_1\right) \tag{34}$$

with

$$\theta\left(I, I_1, I', I'_1\right) = (1 - 1/Z)\delta\left(I - I'\right)\delta\left(I_1 - I'_1\right) + 6\left(1 - I - I'_1\right)/Z \tag{35}$$

and $I = I/E$. The strength of translational-rotational coupling is determined by the mixing parameter Z which can be made to depend on the local flow field temperature to fit experimental relaxation rates [34].

As mentioned above, the hard sphere collision cross section has been used in the DSMC simulations presented in this work. The choice is suggested by the limited temperature range of the experimental measurements which allow to assume a constant value of the total collision cross section. For the same reason, a similar choice has been made about the rotational collision number, Z, whose value has been assumed not to depend on temperature, neglecting its weak temperature dependence in the case of air species [34].

Steady solutions of Eq. (1) have been obtained as the long time limit of unsteady solutions numerically computed by a DSMC scheme [23] in which $f(\hat{\boldsymbol{r}}, \boldsymbol{v}, I, t)$ is represented by a large number of mathematical particles. Each of them is characterized by spatial position $\hat{\boldsymbol{r}}(t)$, velocity $\boldsymbol{v}(t)$ and internal energy $I(t)$ associated with j rotational degrees of freedom. The particles states are advanced from time t to time $t + \Delta t$ in two stages. In the first stage gas–gas collisions are neglected and particles move along straight lines with the constant velocity and rotational energy they had at time t. In this free flight stage wall boundary conditions are applied to change the velocity and internal energy of molecules hitting a wall. In the second stage, particles positions are kept fixed and equal to the final values resulting from the free flight. Particles belonging to the same cell of the spatial grid are allowed to collide according to the rule described above. Macroscopic quantities are obtained by sampling and time averaging particles microscopic states after the onset of steady flow conditions.

In the particular DSMC implementation adopted here, the spatial annular domain $\Re = \{(x, y) : R_A^2 < x^2 + y^2 < R_B^2\}$ is divided into a number of annular cells. Flow properties are assumed not to depend on the coordinate z along the common cylinders axis, hence the z component of particles positions is not used in the advection sub-step. An axisymmetric solution is constructed by converting the global Cartesian x and y components of particles velocities to local radial and transversal components before each collision step. Then, particles within the same annular cell are allowed to collide, irrespectively of their spatial position. After the collision stage is completed, radial and transversal velocity components are converted back to global Cartesian components to perform the next free flight step. Full accommodation has been assumed to occur at both walls.

The reported DSMC results have been obtained from simulations using 10^6 particles and not less than 1250 particles per cell. The statistical errors associated with the heat flux values in Table 2 have been estimated by repeating each simulation eight times, changing the random number sequence. For each of the considered flow conditions, the obtained standard deviation, normalized to the average heat flux value, never exceeds 0.5%, being around 0.2% in most of the computed cases. Cell size Δr not exceeding 1/20 of the reference mean free path has been used. The time step Δt has been set equal to the minimum between the estimated time a particle takes to cross a cell, $(\Delta t)_{adv} = \Delta r/\sqrt{RT_A}$, and a small fraction (typically 1/10) of the minimum mean free time, based on the maximum value v_c of the collision frequency in the domain. Macroscopic quantities have been obtained by sampling microscopic particles states for $20 - 40 \times 10^4$ time steps after the estimated onset of steady conditions. When simulating experimental conditions, where the ratio R_B/R_A takes a very high value, a weighted particle scheme [23] has been used to increase the accuracy near the internal cylinder surface, while keeping the overall number of particles within reasonable limits.

5. Results and discussion

Results for the macroscopic quantities obtained by the Holway and Rykov kinetic models as well as by the DSMC method in a wide range of all parameters involved in the problem are presented in tabulated and graphical form. More specifically, the density, temperature and heat flux distributions are provided for diatomic and polyatomic gases enclosed between cylinders with the normalized temperature difference $\beta = [0.1, 1, 10]$, the radii ratio $\gamma = \left[\frac{1}{2}, \frac{1}{10}, \frac{1}{65}, \frac{1}{667}\right]$ and the gas rarefaction parameter δ_B varying from the free molecular limit up to the hydrodynamic regime. Comparisons between computational results as well as with experimental data are performed.

In Table 1, the dimensionless translational and rotational heat fluxes computed by the Holway and Rykov models ($j = 2$) are given for various β and δ_B with $\gamma = 1/2$. The tabulated results are at the surface $r = \gamma$ of the inner cylinder. The enclosed gas is nitrogen (N_2) and the variable hard sphere (VHS) model with $\omega = 0.74$ has been applied. In the case of the Rykov model, the parameters in Eq. (21) are set to $\omega_0 = 0.2354$, $\omega_1 = 0.3049$ and $\kappa = 0.645$ [31,35]. Results are provided for $Z = 1$ and 5, which are indicative for this type of simulations since as noted in Section 3, $Z = 1$ means that only inelastic collisions occur, while $Z = 5$ refers to the situation where the amount of inelastic collisions is small compared to the elastic ones. In the last column the corresponding heat fluxes obtained by the Shakhov model for a monatomic gas are given. It is observed that the agreement between the results of the Holway and Rykov models is, in general, very good. As expected, at $\delta_B = 0$

identical results are provided and then as δ_B is increased the deviation between the Holway and Rykov heat fluxes is increased. Also, in terms of the parameter Z the agreement is better as Z is increased. The largest discrepancies are about 10% and they are occurring at $Z = 1$ and $\delta_B = 10$ (independent of β). In both models the rotational heat fluxes are about half of the corresponding translational ones (at $\delta_B = 0$, q_{rot} is exactly one-half of q_{tr}). It is clearly seen that the Rykov model is more sensitive to the variation of Z, compared to the Holway model which, at least for this set of parameters, is slightly affected and only at large values of δ_B. In both models as Z is increased, the translational heat fluxes are increased approaching those of the Shakhov model ($Z \to \infty$). The values of q_{tr}, at $Z = 5$, are already close enough to the corresponding $q^{(S)}$. The total heat fluxes $q = q_{tr} + q_{rot}$ of N_2 for the Rykov and Holway models are higher about 22–50% and 36–50% respectively than the corresponding monatomic heat fluxes. It is noted that the analytical free molecular results (see Eqs. (A5) and (A6), with $j = 2$) are recovered to all significant figures tabulated, while the conservation Eq. (29) are fully satisfied. The heat flux distributions between the cylinders are readily reduced by multiplying the tabulated values by the ratio r/γ.

In Table 2, a comparison between the results obtained by the Holway model and the DSMC method for a diatomic gas ($j = 2$) enclosed between cylinders with $\gamma = 1/2$ and various values of β and δ_0 is performed. Based on the hard sphere (HS) model the dimensionless translational and rotational heat fluxes for $Z = 1$ and 5 at $r = \gamma$ are provided. It is important to note that in order to facilitate comparison between the DSMC and kinetic results, the gas rarefaction parameter δ_0 is defined in terms of a reference pressure P_0 given by $P_0 = n_0 k_B T_B$ (instead of $P_B = n_B k_B T_B$), where n_0 is an average reference number density defined as $n_0 = \frac{2}{R_B^2 - R_A^2} \int_{R_A}^{R_B} n(\hat{r}) \hat{r} d\hat{r}$. Therefore, the Holway kinetic heat fluxes presented in Table 2 are not directly compatible with the ones in Table 1. The variation of the DSMC heat fluxes in terms of the problem parameters (β, δ_0, Z) is exactly the same as for the kinetic models. More importantly, in all cases the quantitative agreement between the Holway and DSMC results is excellent with the largest discrepancies not to exceed 5%. For completeness purposes the monatomic modeling results based on the Shakhov model are also included.

The comparison is continued in Figs. 1 and 2, where the distributions of density and temperature respectively, obtained by the Holway and DSMC approaches, are plotted for the indicative values of $\beta = 0.1, 1, 10$ and $\delta_0 = 0.2, 2, 20$. As it is observed in Fig. 1, the corresponding density distributions are in excellent agreement for all β and δ_0, with the relative plots actually coinciding on each other. Furthermore, in Fig. 2 the agreement between the corresponding translational and rotational temperature distributions is again very good in all cases with an exception at $\beta = 10$ and $\delta_0 = 20$, where a small deviation between the relative plots is observed. It is also seen that the translational and rotational temperatures for the same set of parameters are almost identical. Therefore, Eq. (25) yields $\tau \approx \tau_{tr} \approx \tau_{rot}$. Observing the results presented so far (Tables 1 and 2 and Figs. 1 and 2) it is deduced that the deterministic modeling based on two different kinetic model equations namely the Holway and Rykov models and the stochastic modeling based on the DSMC method provide similar results in simulating polyatomic gas heat transfer between coaxial cylinders in a wide range of problem parameters.

Next, a comparison with experimental data available in the literature is performed in terms of the total heat fluxes. In [20], in an effort to estimate the energy accommodation coefficient of various gases, a detailed experimental investigation has been performed for heat transfer in rarefied gases between coaxial cylinders maintained at a very small temperature difference. It has been found that in the case of N_2 the interaction with the wall is almost purely diffusive. These dimensionless experimental data for N_2 with $\gamma = 1/65$ and $T_B = 300$ K (see Tables 2 and 3 in [20]) are compared, in Fig. 3, with the corresponding computational ones, based on the Rykov model. Since the temperature difference is very small and to avoid introducing a specific temperature difference, the linearized Rykov model [35] has been applied. It is noted that the nonlinear Rykov model with $\beta < 0.1$ provides very similar results with those of its linearized version. Simulations are performed with (i) $Z = 3$ and (ii) Z obtained by the Landau-Teller expression [23] based on the Lordi and Mates [36] experimental data and as it is seen in Fig. 3, the corresponding results are in excellent agreement. They are also in very good agreement with the experimental results in a wide range of the gas rarefaction $\delta_B \in [1, 10^2]$. On the contrary, the heat fluxes obtained by the linearized Shakhov kinetic model, also shown in Fig. 3, are erroneous underestimating the experimental ones about 50%.

A comparison with the experimental data in [22] is also performed in Fig. 4, in dimensional form. Now, the inner diameter is $R_A = 75 \mu m$, the radius ratio $\gamma = 1/667$, the temperature of the outer cylinder $T_B = 298$ K and the temperature difference $\Delta T = 100$ K ($\beta = 0.336$). The computational total heat fluxes, based on the

Table 1
Heat fluxes at the inner hot cylinder ($r = \gamma$) with $\gamma = 1/2$ for N_2 ($\omega = 0.74$, $j = 2$, Pr = 0.71) based on the Holway and Rykov models.

β	δ_B	$Z = 1$				$Z = 5$				$q^{(S)}$
		q_{tr}		q_{rot}		q_{tr}		q_{rot}		
		Rykov	Holway	Rykov	Holway	Rykov	Holway	Rykov	Holway	Shakhov
0.1	0	5.64(−2)	5.64(−2)	2.82(−2)	2.82(−2)	5.64(−2)	5.64(−2)	2.82(−2)	2.82(−2)	5.64(−2)
	0.1	5.57(−2)	5.58(−2)	2.78(−2)	2.79(−2)	5.58(−2)	5.58(−2)	2.79(−2)	2.79(−2)	5.59(−2)
	1	4.97(−2)	5.10(−2)	2.46(−2)	2.52(−2)	5.12(−2)	5.11(−2)	2.54(−2)	2.52(−2)	5.15(−2)
	4	3.65(−2)	3.96(−2)	1.75(−2)	1.90(−2)	3.98(−2)	3.97(−2)	1.92(−2)	1.89(−2)	4.08(−2)
	10	2.37(−2)	2.72(−2)	1.11(−2)	1.27(−2)	2.75(−2)	2.74(−2)	1.28(−2)	1.25(−2)	2.87(−2)
1	0	5.64(−1)	5.64(−1)	2.82(−1)	2.82(−1)	5.64(−1)	5.64(−1)	2.82(−1)	2.82(−1)	5.64(−1)
	0.1	5.57(−1)	5.58(−1)	2.78(−1)	2.79(−1)	5.59(−1)	5.58(−1)	2.79(−1)	2.79(−1)	5.60(−1)
	1	4.98(−1)	5.11(−1)	2.47(−1)	2.53(−1)	5.14(−1)	5.11(−1)	2.56(−1)	2.53(−1)	5.18(−1)
	4	3.73(−1)	4.01(−1)	1.81(−1)	1.94(−1)	4.05(−1)	4.02(−1)	1.97(−1)	1.93(−1)	4.15(−1)
	10	2.53(−1)	2.86(−1)	1.20(−1)	1.35(−1)	2.90(−1)	2.88(−1)	1.37(−1)	1.34(−1)	3.02(−1)
10	0	5.64	5.64	2.82	2.82	5.64	5.64	2.82	2.82	5.64
	0.1	5.57	5.58	2.79	2.79	5.61	5.58	2.81	2.79	5.62
	1	5.00	5.10	2.49	2.53	5.24	5.10	2.62	2.53	5.31
	4	3.86	4.08	1.91	2.00	4.25	4.08	2.11	2.00	4.37
	10	2.86	3.10	1.40	1.51	3.24	3.11	1.59	1.50	3.37

Table 2
Heat fluxes at the inner hot cylinder ($r = \gamma$) with $\gamma = 1/2$ for a diatomic gas ($j = 2$, Pr = 0.71) with HS molecules, based on the Holway model and the DSMC method.

| β	δ_0	$Z = 1$				$Z = 5$				$q^{(S)}$
		q_{tr}		q_{rot}		q_{tr}		q_{rot}		
		Holway	DSMC	Holway	DSMC	Holway	DSMC	Holway	DSMC	Shakhov
0.1	0.2	5.59(−2)	5.61(−2)	2.79(−2)	2.80(−2)	5.59(−2)	5.62(−2)	2.79(−2)	2.79(−2)	5.61(−2)
	2	4.73(−2)	4.81(−2)	2.30(−2)	2.36(−2)	4.73(−2)	4.89(−2)	2.30(−2)	2.30(−2)	4.81(−2)
	8	3.08(−2)	3.09(−2)	1.44(−2)	1.49(−2)	3.09(−2)	3.26(−2)	1.42(−2)	1.40(−2)	3.23(−2)
	20	1.79(−2)	1.76(−2)	8.18(−3)	8.30(−3)	1.81(−2)	1.89(−2)	8.03(−3)	7.76(−3)	1.93(−2)
1	0.2	5.98(−1)	6.01(−1)	2.98(−1)	3.00(−1)	5.98(−1)	6.02(−1)	2.98(−1)	2.99(−1)	6.01(−1)
	2	5.16(−1)	5.26(−1)	2.52(−1)	2.59(−1)	5.17(−1)	5.35(−1)	2.52(−1)	2.53(−1)	5.30(−1)
	8	3.42(−1)	3.45(−1)	1.61(−1)	1.66(−1)	3.44(−1)	3.62(−1)	1.59(−1)	1.57(−1)	3.60(−1)
	20	2.03(−1)	2.01(−1)	9.35(−2)	9.53(−2)	2.05(−1)	2.14(−1)	9.18(−2)	8.94(−2)	2.18(−1)
10	0.2	6.85	6.85	3.42	3.42	6.85	6.85	3.42	3.41	7.00
	2	6.48	6.64	3.19	3.26	6.48	6.65	3.17	3.17	6.99
	8	4.85	4.94	2.32	2.38	4.86	5.06	2.29	2.24	5.27
	20	3.26	3.27	1.53	1.56	3.29	3.43	1.50	1.46	3.54
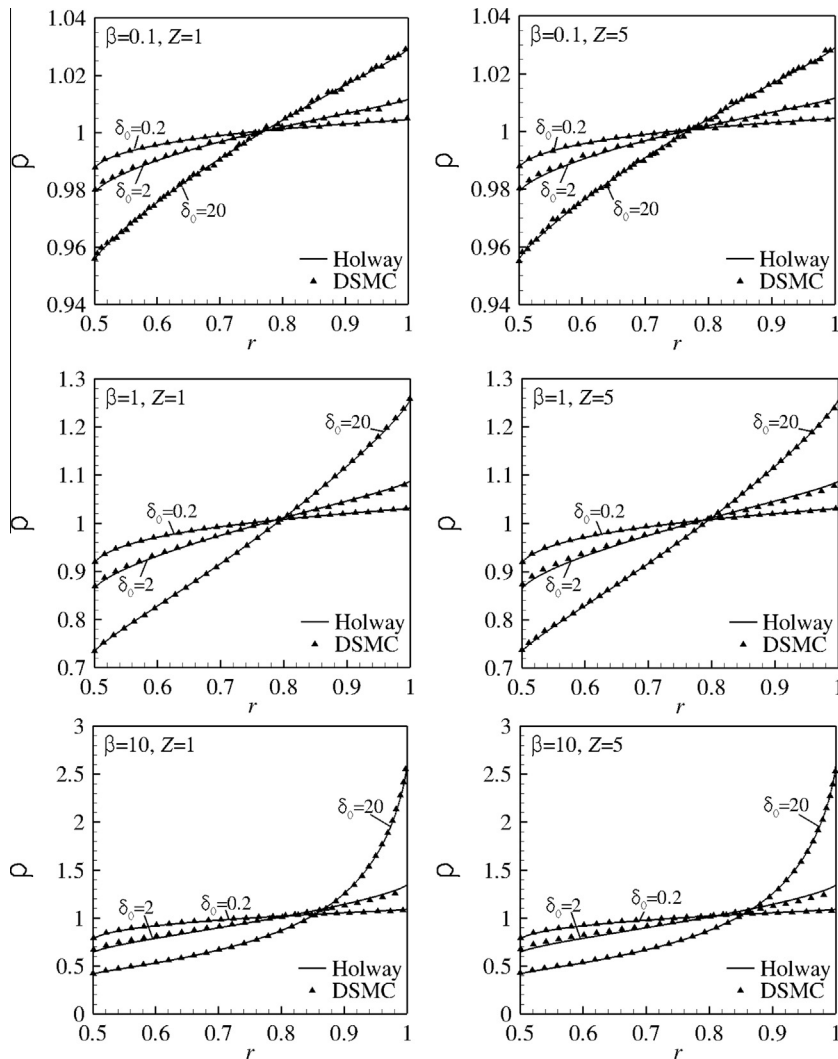
Fig. 1. Dimensionless density distributions with $\gamma = 1/2$ for a diatomic gas ($j = 2$, Pr = 0.71) with HS molecules, based on the Holway model and the DSMC method.

DSMC method and the Rykov model, with $Z = 3$, are in very good agreement with the experimental ones, while once again the heat fluxes based on the Shakhov model for monatomic gases are significantly smaller than the experimental ones. As it is seen the comparison is in a wide range of the reference pressure P_B varying from 1 Pa up to 10^3Pa, with the corresponding gas rarefaction parameter δ_B varying from 6 up to 2,600. It is noted that as δ_B is increased the computational results tend to the analytical ones obtained by
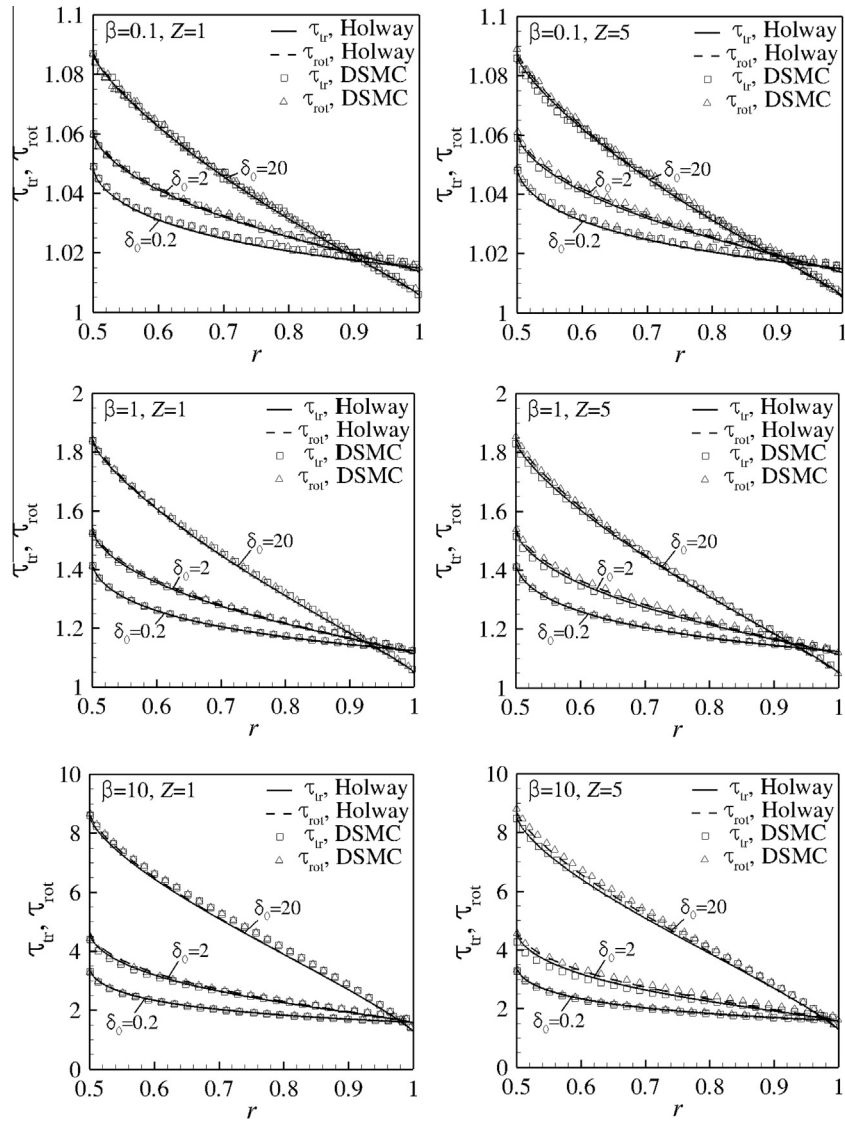
Fig. 2. Dimensionless translational and rotational temperature distributions with $\gamma = 1/2$ for a diatomic gas ($j = 2$, Pr = 0.71) with HS molecules, based on the Holway model and the DSMC method.

Eq. (A9). Indicative simulations performed with Z obtained by the Landau-Teller expression are, once again, in very good agreement with the ones for $Z = 3$. Overall, the comparison studies in Figs. 3 and 4 with the experimental data in [20,22] respectively, validate the simulation results.

In Table 3, the translational, rotational and total heat fluxes of a diatomic gas ($j = 2$) are presented for $\gamma = \left[\frac{1}{2}, \frac{1}{10}, \frac{1}{65}\right]$, $\beta = [0.1, 1, 10]$ and $\delta_B = [0, 0.1, 1, 4, 10]$. These dimensionless results demonstrate the effect of all parameters on the heat fluxes including the effect of the radius ratio, which has not been shown before. Furthermore, they may be used for reference purposes in future computational and experimental studies. Therefore, in order to be as general as possible for diatomic gases, they are obtained based on the Holway model, which depends only on the parameter Z. Also, based on the literature the value of $Z = 3$ used in the simulations, is the most suitable one covering a wide range of diatomic gases. The behavior of the polyatomic heat fluxes in terms of γ, β and δ_B, qualitatively is similar to that of the monatomic ones (are also included for comparison purposes), i.e., they are increased slowly as γ is decreased, they are increased almost proportionally to β and they are decreased as δ_B is increased. Quantitatively however, they vary

significantly, with the polyatomic heat fluxes being 36–50% higher. Also, q_{rot} is about one-half of q_{tr}, with the latter one to be close and always smaller to $q^{(S)}$.

In Table 4, the translational, rotational and total heat fluxes for a polyatomic gas ($j = 3$) are presented for $\gamma = 1/2$, $\beta = [0.1, 1, 10]$ and $\delta_B = [0, 0.1, 1, 4, 10]$. The results are based on the Holway model and since no results for $j = 3$ have been presented so far, the parameter Z is set to $Z = 1$ and 5. The variation of all heat fluxes in terms of β and δ_B, as well as of Z I similar to the one for a diatomic gas (see Tables 1 and 2). The numerical solutions at $\delta_B = 0$ are exactly the same to all tabulated significant figures with the ones obtained by the analytical expressions (A6) with $j = 3$. Also, at $\delta_B = 0$, q_{rot} is 75% (instead of 50%) of q_{tr}. This relation applies approximately to all $\delta_B > 0$ independent of β, with rotational heat fluxes to be about 75% of the translational ones, while the latter ones are close to the translational heat fluxes of a diatomic (and monatomic) gas. As a result the dimensionless total heat fluxes of polyatomic gases are about 58–75% higher than the corresponding monatomic ones.

In order to obtain a more physical understanding of the heat transfer in monatomic and polyatomic gases and to facilitate comparisons with experiments, in Fig. 5, some dimensional total heat
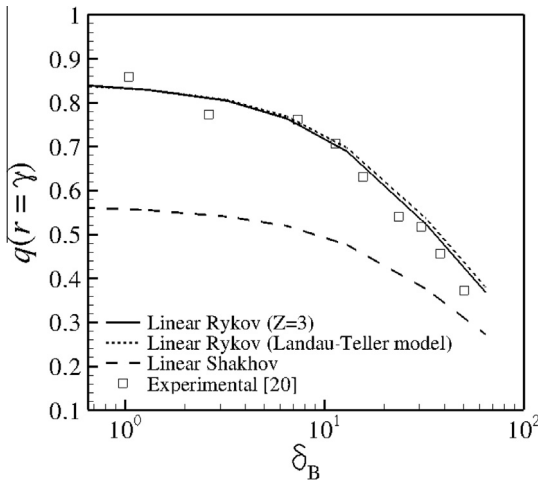
Fig. 3. Comparison between computational and experimental [20] dimensionless heat fluxes q ($r = \gamma$) for N_2 confined between two cylinders with R_A = 200 μm, 1/65 and maintained at a very small temperature difference with T_B = 300 K.
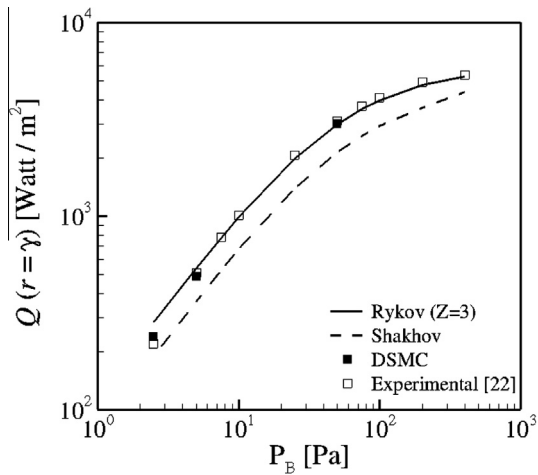

Fig. 4. Comparison between computational and experimental [22] dimensional heat fluxes $Q(r = \gamma)$ for N_2 and air respectively, confined between two cylinders with R_A = 75 μm, γ = 1/667 and maintained at a temperature difference of ΔT = 100 K, with T_B = 298 K.

Table 3
Heat fluxes at the inner hot cylinder ($r = \gamma$) for a diatomic gas ($j = 2$, Pr = 0.71) with HS molecules.

γ	β	δ_B	Holway(Z = 3)			Shakhov
			q_{tr}	q_{rot}	q	$q^{(S)}$
1/2	0.1	0	5.64(−2)	2.82(−2)	8.46(−2)	5.64(−2)
		0.1	5.58(−2)	2.79(−2)	8.37(−2)	5.59(−2)
		1	5.10(−2)	2.51(−2)	7.62(−2)	5.15(−2)
		4	3.95(−2)	1.88(−2)	5.84(−2)	4.07(−2)
		10	2.72(−2)	1.25(−2)	3.97(−2)	2.86(−2)
	1	0	5.64(−1)	2.82(−1)	8.46(−1)	5.64(−1)
		0.1	5.58(−1)	2.79(−1)	8.37(−1)	5.59(−1)
		1	5.09(−1)	2.51(−1)	7.60(−1)	5.15(−1)
		4	3.95(−1)	1.90(−1)	5.84(−1)	4.08(−1)
		10	2.77(−1)	1.29(−1)	4.06(−1)	2.91(−1)
	10	0	5.64	2.82	8.46	5.64
		0.1	5.57	2.78	8.35	5.62
		1	4.99	2.48	7.47	5.22
		4	3.84	1.87	5.71	4.11
		10	2.81	1.35	4.15	3.04
1/10	0.1	0	5.64(−2)	2.82(−2)	8.46(−2)	5.64(−2)
		0.1	5.61(−2)	2.80(−2)	8.41(−2)	5.61(−2)
		1	5.32(−2)	2.64(−2)	7.96(−2)	5.38(−2)
		4	4.51(−2)	2.19(−2)	6.70(−2)	4.66(−2)
		10	3.41(−2)	1.62(−2)	5.04(−2)	3.62(−2)
	1	0	5.64(−1)	2.82(−1)	8.46(−1)	5.64(−1)
		0.1	5.61(−1)	2.80(−1)	8.41(−1)	5.62(−1)
		1	5.30(−1)	2.63(−1)	7.93(−1)	5.39(−1)
		4	4.45(−1)	2.17(−1)	6.62(−1)	4.63(−1)
		10	3.37(−1)	1.61(−1)	4.98(−1)	3.57(−1)
	10	0	5.64	2.82	8.46	5.64
		0.1	5.60	2.80	8.40	5.66
		1	5.22	2.60	7.82	5.61
		4	4.21	2.08	6.29	4.70
		10	3.17	1.55	4.72	3.50
1/65	0.1	0	5.64(−2)	2.82(−2)	8.46(−2)	5.64(−2)
		0.1	5.63(−2)	2.82(−2)	8.45(−2)	5.63(−2)
		1	5.55(−2)	2.77(−2)	8.32(−2)	5.57(−2)
		4	5.29(−2)	2.62(−2)	7.91(−2)	5.35(−2)
		10	4.80(−2)	2.36(−2)	7.17(−2)	4.94(−2)
	1	0	5.64(−1)	2.82(−1)	8.46(−1)	5.64(−1)
		0.1	5.63(−1)	2.82(−1)	8.45(−1)	5.64(−1)
		1	5.55(−1)	2.77(−1)	8.31(−1)	5.58(−1)
		4	5.25(−1)	2.60(−1)	7.85(−1)	5.34(−1)
		10	4.70(−1)	2.32(−1)	7.02(−1)	4.87(−1)
	10	0	5.64	2.82	8.46	5.64
		0.1	5.63	2.82	8.45	5.65
		1	5.52	2.76	8.27	5.70
		4	5.07	2.52	7.59	5.50
		10	4.32	2.14	6.47	4.75

fluxes [W/m^2] in terms of the reference pressure P_B [Pa] are given for the monatomic gases of He and Ar, the diatomic gases of H_2 and N_2 and for the polyatomic gas of CO_2. The inner diameter is R_A = 1 cm with $\gamma = \left[\frac{1}{2}, \frac{1}{10}\right]$, while the reference temperature is T_B = 293 K with β = [0.1,1]. The reference pressure $P_B \in [10^{-3},10]$Pa and is easily connected to the rarefaction parameter δ_B, via Eq. (6) once the viscosity and the most probable velocity of each gas is specified. All computations are based on the Holway model with $Z = 3$ and the VHS model (ω = [0.66,0.81,0.67,0.74,0.93] for He, Ar, H_2, N_2, CO_2 respectively). In all cases, as expected, the heat flux is monotonically increased with pressure. At highly rarefied atmospheres the heat flux is proportional to gas pressure, then, in the transition regime the relation becomes more complex and at dense atmospheres the heat flux depends weakly and finally is independent of pressure. Also, the heat fluxes for β = 1 are about one order magnitude higher than the corresponding ones for β = 0.1, while the effect of γ is not that important with the heat fluxes to be slightly decreased as the gap between the cylinders is increased.

More importantly, it is observed in Fig. 5, that under the same conditions the heat flux of different gases varies significantly. The largest heat fluxes are achieved for H_2 followed successively by the heat fluxes of He, N_2, CO_2 and Ar. This trend is valid in the whole range of pressure except for the curves of CO_2 and Ar, which cross each other at some relatively large pressure P_B > 1 Pa. It is well known that in heat transfer through monatomic gases confined between coaxial cylinders, the dimensional heat flux is increased as the molar mass of the gas is decreased (see Fig. 9 in [2]). However, this remark cannot be generalized in the case of polyatomic gases since, as seen in Fig. 5, in a wide range of pressure the heat flux of CO_2 is larger than that of Ar, while its molar mass is larger.

It has been proposed in [18] that the heat flux between confined coaxial cylinders may be computed in the whole range of the rarefaction parameter, assuming small temperature differences and large radius ratios, according to
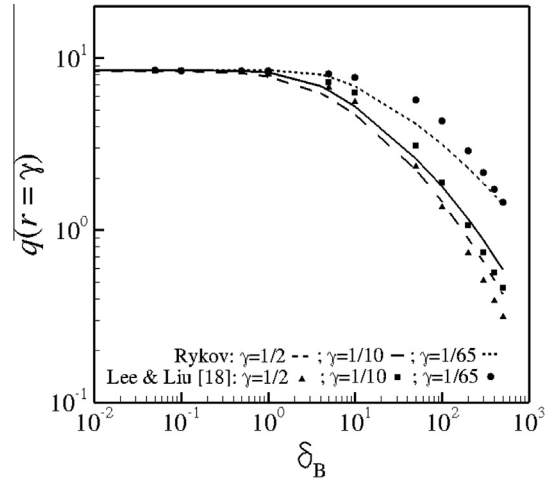
$$\frac{1}{q} = \frac{1}{q_{FM}} + \frac{1}{q_C} \qquad (36)$$

Table 4
Heat fluxes at the inner hot cylinder ($r = \gamma$) with $\gamma = 1/2$ for a polyatomic gas ($j = 3$, Pr = 0.71) with HS molecules based on the Holway model.

β	δ_B	$Z = 1$			$Z = 5$		
		q_{tr}	q_{rot}	q	q_{tr}	q_{rot}	q
0.1	0	5.64(−2)	4.23(−2)	9.87(−2)	5.64(−2)	4.23(−2)	9.87(−2)
	0.1	5.58(−2)	4.18(−2)	9.76(−2)	5.58(−2)	4.18(−2)	9.76(−2)
	1	5.10(−2)	3.77(−2)	8.87(−2)	5.10(−2)	3.77(−2)	8.87(−2)
	4	3.94(−2)	2.83(−2)	6.77(−2)	3.96(−2)	2.82(−2)	6.78(−2)
	10	2.70(−2)	1.88(−2)	4.58(−2)	2.72(−2)	1.86(−2)	4.58(−2)
1	0	5.64(−1)	4.23(−1)	9.87(−1)	5.64(−1)	4.23(−1)	9.87(−1)
	0.1	5.58(−1)	4.18(−1)	9.76(−1)	5.58(−1)	4.18(−1)	9.76(−1)
	1	5.08(−1)	3.77(−1)	8.86(−1)	5.09(−1)	3.77(−1)	8.86(−1)
	4	3.94(−1)	2.85(−1)	6.79(−1)	3.95(−1)	2.84(−1)	6.79(−1)
	10	2.76(−1)	1.94(−1)	4.70(−1)	2.77(−1)	1.92(−1)	4.69(−1)
10	0	5.64	4.23	9.87	5.64	4.23	9.87
	0.1	5.57	4.17	9.74	5.57	4.17	9.74
	1	4.99	3.72	8.71	4.99	3.72	8.71
	4	3.82	2.82	6.64	3.84	2.81	6.65
	10	2.79	2.03	4.82	2.81	2.01	4.82

Fig. 6. Comparison of the radial heat flux at the inner hot cylinder $q(r = \gamma)$ for N_2 and $\beta = 10$ with corresponding results of Eq. (36).

where q_{FM} and q_C are the corresponding free molecular and continuum heat fluxes, which are readily obtained by Eqs. (A6) and (A9). It has been observed in [3] that in monatomic gases this expression remains valid well beyond the introduced assumptions providing easy-to-go results. Here, this investigation is extended to N_2 and in Fig. 6, a comparison is made between the computed heat fluxes based on the Rykov model for the large temperature difference of $\beta = 10, \gamma = \left[\frac{1}{2}, \frac{1}{10}, \frac{1}{65}\right]$ and in a wide range of δ_B, with the corresponding

ones obtained by the empirical Eq. (36). It is seen that the agreement is excellent for $\delta_B < 10$ and then as δ_B is further increased there are some discrepancies which are increased as γ is decreased. However, the overall agreement remains good and it becomes even better as β is decreased. Therefore this expression may also be implemented in polyatomic gases for engineering purposes when the temperature distributions are not needed.
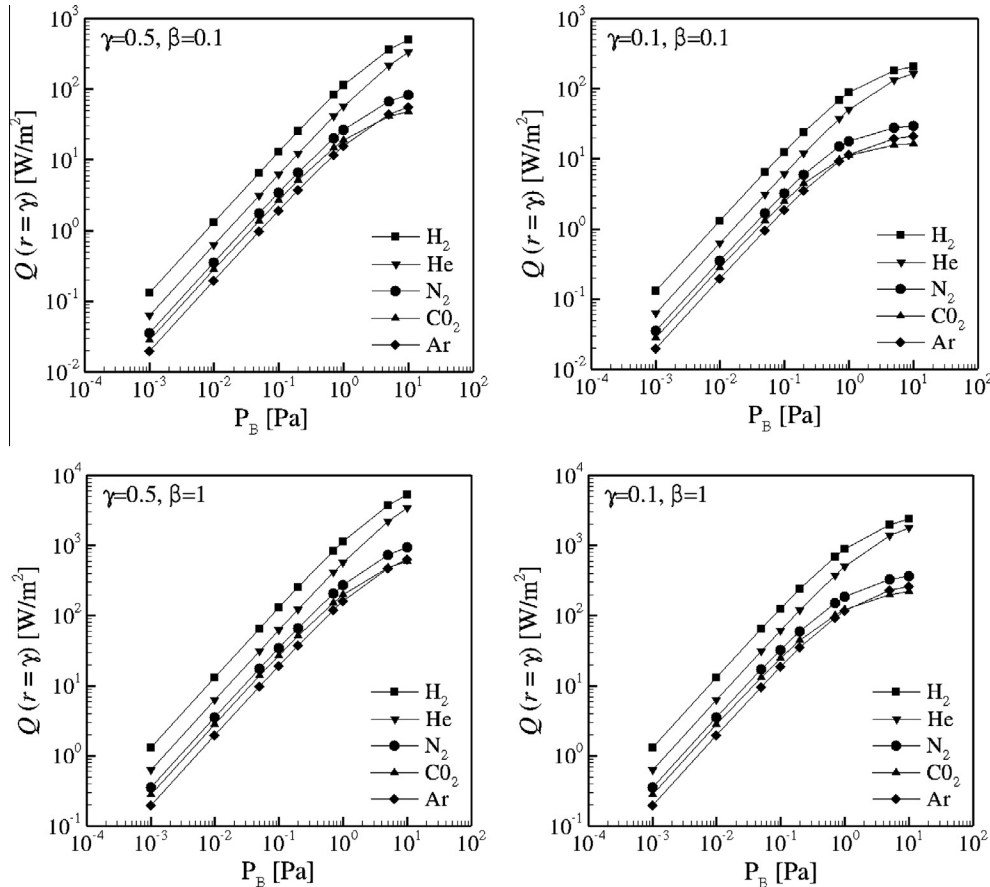
Fig. 5. Dimensional heat flux $Q(r = \gamma)$ through various gases enclosed between two cylinders with $R_A = 1$ cm and $\gamma = [1/2, 1/10]$, maintained at $T_B = 293$ K and $\beta = [0.1, 1]$, in terms of the reference pressure P_B obtained by the Holway model ($Z = 3$, VHS model).

6. Concluding remarks

The problem of heat transfer through rarefied polyatomic gases confined between two coaxial cylindrical surfaces maintained at different temperatures is solved based on the Holway and Rykov kinetic models as well as on the DSMC method subject to the Borgnakke - Larsen collision model. The quantitative behavior of the radial heat flux is examined in a wide range of the gas rarefaction parameter, small, moderate and large normalized temperature differences and various radius ratios. The deduced density and temperature (translational, rotational, total) distributions are also provided. The results obtained by the two kinetic models are in good agreement, with the Rykov model being more sensitive, compared to the Holway model, in the variation of the mixing parameter indicating the strength of translational-rotational coupling. Very good agreement between the Holway model and DSMC results for HS molecules has also been observed. In addition, the computational results perfectly match the analytical ones in the free molecular and continuum limits. These findings along with the successful comparison between simulations and available experimental data for polyatomic gases associated to small and large temperature differences demonstrate the validity of the implemented modeling approaches.

The translational and rotational as well as the total temperatures are very close to each other for all parameters examined here and they are similar to the corresponding monatomic ones. In contrary, the total heat fluxes for polyatomic gases are significantly higher than those for monatomic gases. More specifically, the heat fluxes of diatomic and polyatomic gases, obtained by the Holway model, are higher about 36–50% and 58–75% respectively than the corresponding ones obtained by the Shakhov model, with the highest differences occurring in the free molecular limit. As the amount of elastic compared to inelastic collisions is increased, the translational heat fluxes are increased and they tend to the monatomic ones, while always the rotational heat fluxes are about 50% and 75% of the translational ones for diatomic and polyatomic gases respectively. Furthermore, it has been found that the simple expression (36), proposed in [18], provides reasonably accurate results in a wide range of parameters, while another observation of practical interest is that, while in monatomic the dimensional heat flux is increased as the molar mass is decreased, this is not necessarily the case in polyatomic gases.

Overall, it may be stated that the implementation of the Holway model is more flexible to polyatomic gases, while the Rykov model, although seems to be more accurate, is limited to diatomic gases and additional experimental data for the specific gas under consideration. In addition, since polyatomic kinetic modeling provides heat fluxes, which are significantly higher than the corresponding monoatomic ones, heat transfer simulations in MEMS and other technological devices with polyatomic gases must be based on polyatomic kinetic modeling.

Conflict of Interest

None declared.

Acknowledgments

Appendix A. Analytical solutions in the free molecular and continuum limits

In the free molecular limit ($\delta_B = 0$) the right hand side of Eq. (17) becomes zero and in the case of Maxwell diffuse boundary conditions the reduced distribution functions are given for $\theta \in [-\pi/2, \pi/2]$ by

$$F^{(i)} = \frac{\rho_w^{(i)}}{\pi(1+\beta)} \exp\left[-\frac{\zeta^2}{1+\beta}\right], \quad G^{(i)} = \frac{\rho_w^{(i)}}{\pi} \exp\left[-\frac{\zeta^2}{1+\beta}\right],$$
$$S^{(i)} = \frac{j\rho_w^{(i)}}{2\pi} \exp\left[-\frac{\zeta^2}{1+\beta}\right] \tag{A1}$$

and for $\theta \in [\pi/2, 3\pi/2]$ by

$$F^{(i)} = \frac{1}{\pi} \exp\left[-\frac{\zeta^2}{1+\beta}\right], \quad G^{(i)} = \frac{1}{2\pi} \exp\left[-\frac{\zeta^2}{1+\beta}\right],$$
$$S^{(i)} = \frac{j}{2\pi} \exp\left[-\frac{\zeta^2}{1+\beta}\right] \tag{A2}$$

where the impermeability parameter is found from the no penetration condition to be

$$\rho_w^{(i)} = \frac{1}{\sqrt{1+\beta}} \tag{A3}$$

Then, substituting Eqs. (A1)–(A3) into the moment Eqs. (20)–(26) and following a straightforward manipulation yields

$$\rho^{(i)}(r) = \frac{1}{\pi}\left(\frac{\theta_1}{\sqrt{1+\beta}} - \theta_1 + \pi\right) \tag{A4}$$

$$\tau_{tr}^{(i)}(r) = \tau_{rot}^{(i)}(r) = \frac{1}{\rho^{(i)}(r)\pi}\left[\theta_1\left(\sqrt{1+\beta}\right) + \pi - \theta_1\right] \tag{A5}$$

$$q_{tr}^{(i)}(r) = \frac{\beta\gamma}{r\sqrt{\pi}} \quad q_{rot}^{(i)}(r) = \frac{j\beta\gamma}{4r\sqrt{\pi}} \quad q^{(i)}(r) = \left(1+\frac{j}{4}\right)\frac{\beta\gamma}{r\sqrt{\pi}} \tag{A6}$$

In Eqs. (A4) and (A5), the discontinuity angle θ_1 is given by $\theta_1 = \sin^{-1}(\gamma/r)$. Obviously the results do not depend on the type of model and are exactly the same for the Holway and Rykov models. However, we keep the superscript $i = H, R$ just for consistency in notation.

It is seen that in the free molecular limit for $j = 2$ and $j = 3$ the rotational heat flux is one half and three quarters respectively of the corresponding translational one, while in the case of a monatomic gas ($j = 0$), the rotational is equal to zero and the translational is equal to the total heat flux. It is noted that the numerical solution for $\delta_B = 0$ is in excellent agreement with the analytical results of Eqs. (A3)–(A6).

In the hydrodynamic limit ($\delta_B \to \infty$), based on the Fourier law, the dimensionless heat flux for a monatomic gas with HS molecules confined between two cylinders has been obtained analytically in [2]. It is noted that the ratio of the thermal conductivity λ of a polyatomic gas over its viscosity μ, introducing the Eucken correction, can be written as [37]

$$\frac{\lambda}{\mu} = \frac{9c_p - 5c_v}{4} \tag{A7}$$

where c_p and c_v are the specific heats at constant pressure and temperature respectively given, in terms of the degrees of freedom $j = 0,2,3$, by

$$c_p = \frac{k_B}{m}\frac{5+j}{2} \quad c_v = \frac{k_B}{m}\frac{3+j}{2} \tag{A8}$$

Then, following the same procedure as in [2] it is readily deduced that

$$q(r) = -\left(\frac{5}{4} + \frac{j}{6}\right)\frac{\left[(\beta+1)^{3/2}+1\right]}{r\delta_B \ln\gamma} \tag{A9}$$

For $j = 0$, Eq. (A9) is reduced to the monatomic heat flux in [2], while for $j = 2,3$ the corresponding diatomic and polyatomic heat fluxes are obtained. The present numerical results for large values of the gas rarefaction parameter tend to the analytical results of Eq. (A9).

References

[1] F. Sharipov, G. Bertoldo, Heat transfer through a rarefied gas confined between two coaxial cylinders with high radius ratio, Int. J. Vacuum Sci. Technol. 24 (6) (2006) 2087–2093.

[2] S. Pantazis, D. Valougeorgis, Non-linear heat transfer through rarefied gases between coaxial cylindrical surfaces at different temperatures, Eur. J. Mech. B/ Fluids 29 (2010) 494–509.

[3] H. Yamaguchi, K. Kanazawa, Y. Matsuda, T. Niimi, A. Polikarpov, I. Graur, Investigation on heat transfer between two coaxial cylinders for measurement of thermal accommodation coefficient, Phys. Fluids 24 (2012) 062002.

[4] M. Vargas, S. Stefanov, V. Roussinov, Transient heat transfer flow through a binary gaseous mixture confined between coaxial cylinders, Int. J. Heat Mass Transfer 59 (2013) 302–315.

[5] T.F. Morse, Kinetic model for gases with internal degrees of freedom, Phys. Fluids 7 (2) (1964) 159–169.

[6] L.H. Holway, New statistical models for kinetic theory: methods of construction, Phys. Fluids 9 (9) (1966) 1658–1672.

[7] F.B. Hanson, T.F. Morse, Kinetic models for a gas with internal structure, Phys. Fluids 10 (2) (1967) 345–353.

[8] J.W. Cipolla, Heat transfer and temperature jump in a polyatomic gas, Int. J. Heat Mass Transfer 14 (1971) 1599–1610.

[9] J.T. Lin, D.R. Willis, Kinetic theory analysis of temperature jump in a polyatomic gas, Phys. Fluids 15 (1) (1972) 31–38.

[10] S.K. Hsu, T.F. Morse, Kinetic theory of parallel heat transfer in a polyatomic gas, Phys. Fluids 15 (4) (1972) 584–591.

[11] P. Pazooki, S.K. Loyalka, Heat transfer in a polyatomic gas – I. Plane parallel plates, Int. J. Heat Mass Transfer 28 (11) (1985) 2019–2027.

[12] B. Huang, P.F. Hwang, Test of statistical models for gases with and without internal energy states, Phys. Fluids 16 (4) (1973) 466–475.

[13] V.A. Rykov, A model kinetic equation for a gas with rotational degrees of freedom, Fluid Dyn. 10 (6) (1975) 956–966.

[14] I.N. Larina, V.A. Rykov, Boundary conditions for gases on a body surface, Fluid Dyn. 21 (1986) 795–801.

[15] W.P. Teagan, G.S. Springer, Heat transfer and density-distribution measurements between parallel plates in the transition regime, Phys. Fluids 11 (3) (1968) 497–506.

[16] D.J. Alofs, R.C. Flagan, G.S. Springer, Density distribution measurements in rarefied gases contained between parallel plates at high temperature differences, Phys. Fluids 14 (3) (1971) 529–533.

[17] W.M. Trott, J.N. Castaneda, J.R. Torczynski, M.A. Gallis, D.J. Rader, An experimental assembly for precise measurement of thermal accommodation, Rev. Sci. Instrum. 82 (2011) 0355120.

[18] L. Lee, C.Y. Liu, Kinetic-theory description of conductive heat transfer from a fine wire, Phys. Fluids 5 (10) (1962) 1137–1148.

[19] J.W. Cipolla, T.F. Morse, Kinetic description of cylindrical heat conduction in a polyatomic gas, Phys. Fluids 11 (6) (1968) 1292–1300.

[20] Y.G. Semyonov, S.F. Borisov, P.E. Suetin, Investigation of heat transfer in rarefied gases over a wide range of Knudsen number, Int. J. Heat Mass Transfer 27 (10) (1984) 1789–1799.

[21] S.J. O'shea, R.E. Collins, An experimental study of conduction heat transfer in rarefied polyatomic gases, Int. J. Heat Mass Transfer 35 (12) (1992) 3431–3440.

[22] H. Chalabi, O. Buchina, L. Saraceno, M. Lorenzini, D. Valougeorgis, G.L. Morini, Experimental analysis of heat transfer between a heated wire and a rarefied gas in an annular gap with high diameter ratio, J. Phys.: Conf. Ser. 362 (2012) 012028.

[23] G.A. Bird, Monte Carlo simulation of gas flows, Annu. Rev. Fluid Mech. 10 (1978) 11–31.

[24] C. Borgnakke, P.S. Larsen, Statistical collision model for Monte Carlo simulation of polyatomic gas mixture, J. Comput. Phys. 18 (4) (1975) 405–420.

[25] I. Kuscer, A model for rotational energy exchange in polyatomic gases, Physica A 158 (1989) 784–800.

[26] P.L. Bhatnagar, E.P. Gross, M.A. Krook, A model for collision processes in gases. I. Small amplitude processes in charged and neutral one-component systems, Phys. Rev. 94 (1954) 511–525.

[27] L.H. Holway, Approximation procedure for kinetic theory (Ph.D. thesis), Harvard University, 1963.

[28] E.M. Shakhov, Generalization of the Krook kinetic relaxation equation, Fluid Dyn. 3 (5) (1968). 95–95.

[29] P. Andries, P.L. Tallec, J.P. Perlat, B. Perthame, The Gaussian-BGK model of Boltzmann equation with small Prandtl number, Eur. J. Mech. B/Fluids 19 (2000) 813–830.

[30] A. Frezzotti, A numerical investigation of the steady evaporation of a polyatomic gas, Eur. J. Mech. B/Fluids 26 (2007) 93–104.

[31] I.N. Larina, V.A. Rykov, Kinetic model of the Boltzmann equation for a diatomic gas with rotational degrees of freedom, Comput. Math. Math. Phys. 50 (2010) 2118–2130.

[32] J.O. Hirschfelder, C.F. Curtiss, R.B. Bird, Molecular Theory of Gases and Liquids, Wiley, New York, 1954.

[33] S. Chapman, T.G. Cowling, The Mathematical Theory of Non-Uniform Gases, Cambridge University Press, Cambridge, UK, 1990.

[34] I.J. Wysong, D.C. Wadsworth, Assessment of direct simulation Monte Carlo phenomenological rotational relaxation models, Phys. Fluids 10 (1998) 2983–2994.

[35] V.A. Titarev, E.M. Shakhov, Poiseuille flow and thermal creep in a capillary tube on the basis of the R-Model, Fluid Dyn. 47 (2012) 661–672.

[36] J.A. Lordi, R.E. Mates, Rotational relaxation in nonpolar diatomic gases, Phys. Fluids 13 (2) (1970) 291–308.

[37] J.H. Ferziger, H.G. Kaper, Mathematical Theory of Transport Processes in Gases, North-Holland Publishing Company, Amsterdam, 1972.